







# Indoline CD4-mimetic compounds mediate potent and broad HIV-1 inhibition and sensitization to antibody-dependent cellular cytotoxicity

Christopher J. Fritsch<sup>a,1</sup>, Saumya Anang<sup>b,c,1</sup>, Zhen Gong<sup>d,1</sup> , Mohammadjavad Mohammadi<sup>e</sup> , Jonathan Richard<sup>f,g</sup>, Catherine Bourassa<sup>g</sup>, Kenny T. Severino<sup>h</sup>, Hannah Richter<sup>i</sup>, Derek Yang<sup>a</sup>, Hung-Ching Chen<sup>a</sup>, Ta-Jung Chiu<sup>a</sup>, Michael S. Seaman<sup>h</sup> , Navid Madani<sup>b,c</sup>, Cameron Abrams<sup>e</sup>, Andrés Finzi<sup>f,g</sup>, Wayne A. Hendrickson<sup>d,i,2</sup> , Joseph G. Sodroski<sup>b,c,j,2</sup>, and Amos B. Smith III<sup>a,2</sup>

Contributed by Wayne A. Hendrickson; received December 31, 2022; accepted February 22, 2023; reviewed by Celia A. Schiffer and Carol D. Weiss

**Binding to the host cell receptors, CD4 and CCR5/CXCR4, triggers large-scale conformational changes in the HIV-1 envelope glycoprotein (Env) trimer [(gp120/gp41)<sub>3</sub>] that promote virus entry into the cell. CD4-mimetic compounds (CD4mcs) comprise small organic molecules that bind in the highly conserved CD4-binding site of gp120 and prematurely induce inactivating Env conformational changes, including shedding of gp120 from the Env trimer. By inducing more “open,” antibody-susceptible Env conformations, CD4mcs also sensitize HIV-1 virions to neutralization by antibodies and infected cells to antibody-dependent cellular cytotoxicity (ADCC). Here, we report the design, synthesis, and evaluation of novel CD4mcs based on an indoline scaffold. Compared with our current lead indane scaffold CD4mc, BNM-III-170, several indoline CD4mcs exhibit increased potency and breadth against HIV-1 variants from different geographic clades. Viruses that were selected for resistance to the lead indane CD4mc, BNM-III-170, are susceptible to inhibition by the indoline CD4mcs. The indoline CD4mcs also potently sensitize HIV-1-infected cells to ADCC mediated by plasma from HIV-1-infected individuals. Crystal structures indicate that the indoline CD4mcs gain potency compared to the indane CD4mcs through more favorable  $\pi$ - $\pi$  overlap from the indoline pose and by making favorable contacts with the vestibule of the CD4-binding pocket on gp120. The rational design of indoline CD4mcs thus holds promise for further improvements in antiviral activity, potentially contributing to efforts to treat and prevent HIV-1 infection.**

gp120 | entry inhibitor | structure-based drug design | antiretroviral therapy | antibody-dependent cellular cytotoxicity

HIV-1 establishes persistent infections that, if untreated, lead to life-threatening AIDS. The HIV-1 pandemic represents a significant challenge to global health, with 38 million people currently infected and 1.5 million new infections occurring annually (1). Antiretroviral treatments have extended the lives of infected individuals, but treatment needs to be continued indefinitely to prevent viral rebound in most cases (2). Furthermore, the development of drug-resistant HIV-1 strains and drug side effects can limit effective treatment options (3). To date, practical measures to prevent HIV-1 transmission by antiretroviral drugs or vaccines remain elusive (2, 3). Additional approaches to limit HIV-1 replication would complement ongoing efforts to address these challenges.

Entry of HIV-1 into host cells is mediated by the envelope glycoprotein (Env) trimer, which consists of three gp120 exterior subunits noncovalently associated with three gp41 transmembrane subunits (4–6). As the only virus-specific protein on the surface of virions and infected cells, Env serves as a target for host antibodies (Ab) that neutralize viruses and kill infected cells through antibody-dependent cellular cytotoxicity (ADCC) (7–11). The unliganded Env largely resides in a “closed” pretriggered conformation that resists the binding of potentially neutralizing or ADCC-mediating antibodies elicited during natural infection (12–16). CD4 binding drives Env into more “open” conformations that engage the CCR5/CXCR4 coreceptor, promoting additional Env transitions into a gp41 six-helix bundle that fuses the viral and cell membranes (17–22).

The binding site for CD4 is a conserved Env gp120 structure that is conformationally altered by CD4 binding (23, 24). In turn, CD4 binding creates an internal cavity (the Phe 43 cavity) in Env bounded by well-conserved residues from gp120 and a single phenylalanine residue (Phe 43) from CD4 (Fig. 1 *A* and *B*). CD4-mimetic compounds (CD4mcs) comprise organic small-molecule HIV-1 entry inhibitors that bind in the Phe 43 cavity, as well as occupy the gp120 “vestibule” leading into the cavity (25). Highly conserved gp120 residues in the vestibule make critical contacts with CD4;

## Significance

HIV-1 presents major global health challenges, as prevention of transmission, control of disease progression, and eradication of viral reservoirs remain unmet goals. CD4-mimetic compounds (CD4mcs) mimic the CD4 receptor and prematurely trigger the HIV-1 envelope glycoproteins (Env), leading to inactivation. Previous lead CD4mcs inhibit HIV-1 infection both in tissue culture and animal models; however, these CD4mcs exhibit limited potency against some HIV-1 strains and are ineffective against others. Here, we present indoline CD4mcs with increased potency and breadth of anti-HIV-1 activity, as well as greater ability to sensitize HIV-1-infected cells to antibody-dependent cellular cytotoxicity (ADCC). This study opens new opportunities for the rational design of indoline CD4mcs that may complement current HIV-1 treatment and prevention methods.

Reviewers: C.A.S., University of Massachusetts Medical School; and C.D.W., FDA/CBER.

Competing interest statement: US Provisional Application No. 63 347,477, “Compounds for the treatment of HIV,” patent filed 5-31-2022.

Copyright © 2023 the Author(s). Published by PNAS. This open access article is distributed under [Creative Commons Attribution-NonCommercial-NoDerivatives License 4.0 \(CC BY-NC-ND\)](https://creativecommons.org/licenses/by-nc-nd/4.0/).

<sup>1</sup>C.J.F., S.A., and Z.G. contributed equally to this work.

<sup>2</sup>To whom correspondence may be addressed. Email: wah2@cumc.columbia.edu, smithab@sas.upenn.edu, or joseph\_sodroski@dfci.harvard.edu.

This article contains supporting information online at <https://www.pnas.org/lookup/suppl/doi:10.1073/pnas.2222073120/-/DCSupplemental>.

Published March 24, 2023.

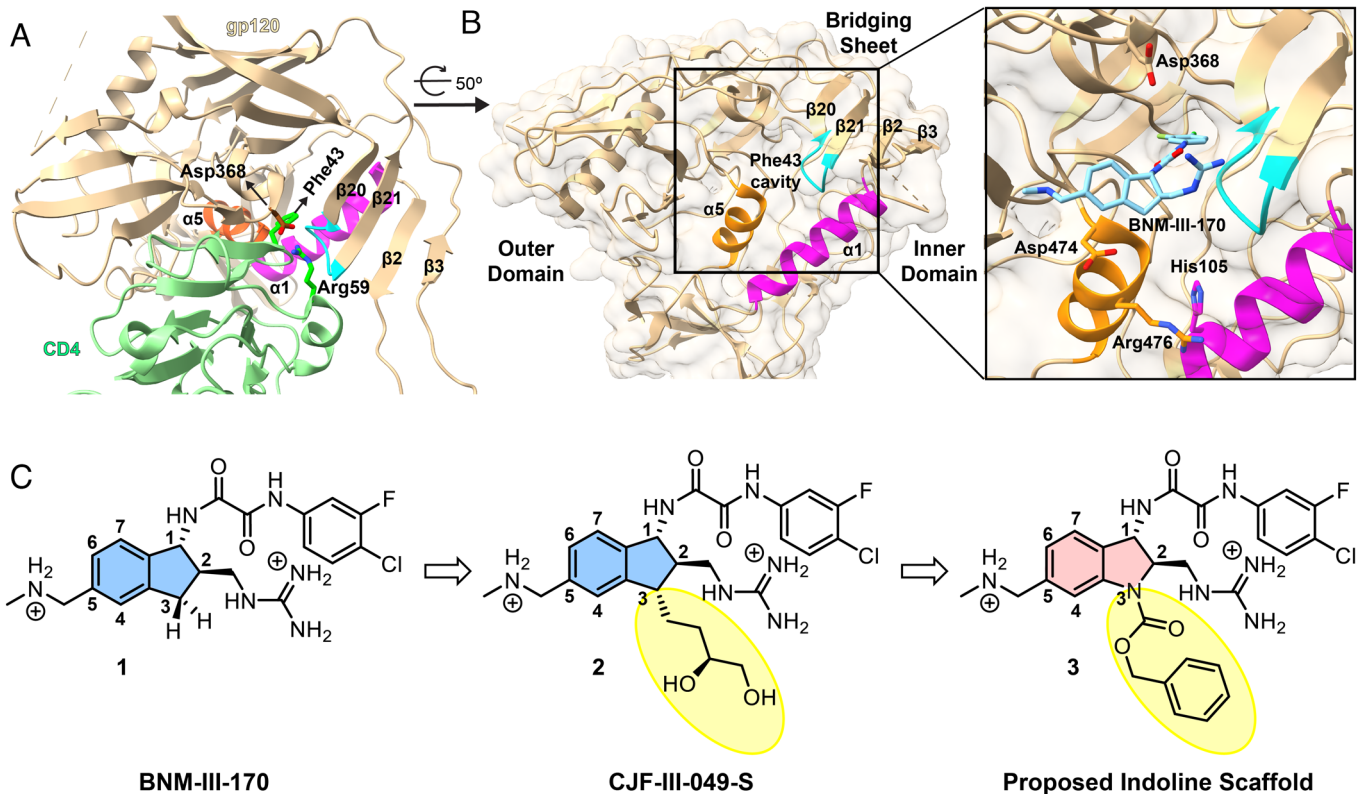


**Fig. 1.** Targeting the Phe 43 cavity and surrounding vestibule of HIV-1 gp120. (A) Interactions between HIV-1<sub>HXBc2</sub> gp120 and CD4 (PDB: 1GC1) are displayed with structural features crucial for CD4 binding highlighted. HIV-1<sub>HXBc2</sub> gp120 and CD4 are shown in beige and light green ribbon diagrams respectively. The  $\alpha 5$  (orange) and  $\alpha 1$  (magenta) helices, as well as the  $\beta 20/21$  loop (cyan), harbor residues that contribute to native CD4 binding. Side chains of Asp368 of gp120 and Arg59 of CD4 are in stick representation to show interactions between gp120 and CD4. Residue Phe43 of CD4 is also depicted reaching into the heart of gp120. The gp120 carbon atoms, CD4 carbon atoms, and oxygen and nitrogen atoms are shown in brown, dark green, red, and blue, respectively. (B) A protomer of HIV-1<sub>BG505</sub> gp120 trimer (PDB: 5THR) is drawn as in A and oriented as indicated. The marked inset shows BNM-III-170, from a complex with HIV-1<sub>C1086</sub> (PDB: 5F4P), in the vestibule of the Phe 43 cavity. Side chains are shown for gp120 residues targeted for CD4mc interaction as in structures with CJF-III-049-S (38) and with CD4 (23). (C) Evolution of more potent CD4mcs from BNM-III-170 (1) (39).

therefore, by occupying the gp120 vestibule, the CD4mcs directly compete with CD4 (26, 27). In addition, CD4mcs prematurely trigger conformational changes in Env similar to those induced by CD4 (26, 28, 29). In the absence of coreceptor-expressing target cells, these prematurely activated Envs rapidly and irreversibly become nonfunctional, in some cases shedding gp120 (28, 29). At concentrations that do not completely inhibit HIV-1 infection, CD4mcs induce open conformations of Env, thereby sensitizing HIV-1 virions to neutralization or HIV-1-infected cells to ADCC by otherwise ineffectual antibodies (30–34). CD4mcs have been shown to synergize with ADCC-mediating antibodies to decrease the HIV-1-infected cell reservoir in humanized mice (35). CD4mcs directly protect humanized mice from vaginal acquisition of HIV-1, and in combination with vaccine-elicited antibodies, CD4mcs protect monkeys from a stringent heterologous simian-human immunodeficiency virus mucosal challenge (36, 37).

Early CD4mcs discovered by Debnath et al. (27) using a gp120-CD4 screen exhibited weak antiviral potency against a limited range of HIV-1 isolates. Replacement of the tetramethyl-piperidine scaffold of these prototypic CD4mcs with an indane scaffold represented a key advance (24, 37). Rationally designed indane CD4mcs (Fig. 1C) were able to achieve more contacts with the gp120 vestibule, resulting in increased antiviral potency and breadth (39). Nonetheless, some primary HIV-1 strains remain resistant even to the most potent indane CD4mc, BNM-III-170 (1). HIV-1 passaged in the presence of BNM-III-170 develops resistance to this CD4mc

as a result of Env changes in the Phe 43 cavity and in a gp120 element that allosterically modulates CD4 binding (40).

The practical utility of CD4mcs as antiviral agents would be enhanced by the availability of more potent analogs with better coverage of HIV-1 strains. Guided by the crystal structures of BNM-III-170 and congeners thereof, we found that 3-substituents on the indane ring of BNM-III-170 can contact a vestibule pocket situated at the interface of the gp120 inner and outer domains, between the  $\alpha 1$  and  $\alpha 5$  helices (Fig. 1B). As a result, some 3-substituted indane analogs, such as CJF-III-049-S (2, Fig. 1C), exhibited modest (threefold) improvements in antiviral activity compared with BNM-III-170; however, only the viruses with His 105 in the gp120  $\alpha 1$  helix showed such an increase (38).

Based on the above observations, we hypothesized that replacing the C3 carbon with nitrogen (Fig. 1C) to create an indoline scaffold might have several benefits. First, the N3 nitrogen of the indoline scaffold would permit facile incorporation of diverse functional groups (vide infra). Second, the nitrogen at N3 would be expected to limit conformational freedom of the five-membered ring, thereby decreasing the number of conformational states that the oxalamide (at C1) and methyl guanidinium (at C2) can adopt. Only one state has been observed by X-ray for the indane CD4mc complexes with gp120 (24, 37, 40), but an entropic penalty would be expected in selecting this pose upon complexation. Lastly, the rigidified five-membered ring of the indolines may lead to different geometries of the substituents at the N3 position, compared to the reported indane congeners (38). This would permit different

branching angles of the substituents, thereby allowing exploration of broader chemical space, given the highly modular nature of the indoline scaffold.

## Results

**A. Synthetic Chemistry.** Based on the rationale above, we set out to design a synthetic route to obtain the indoline CD4mc framework. As illustrated in Fig. 2A, anthranilic ester **4** was first protected as a benzyl carbamate. This was followed by one-pot alkylation with methyl bromoacetate (**5**) and then an intramolecular Claisen condensation employing cesium carbonate to furnish the oxindole **6**.

Judicious choice of the aniline nitrogen protecting group proved important for late-stage functionalization, as we desired to react selectively at this N3 nitrogen in the presence of both the scaffold's guanidinium (at C2) and methylamino methyl (at C5) substituents. Taking inspiration from our process synthesis developed for

BNM-III-170 (**41**), a dynamic kinetic resolution was performed on the oxindole **6** to give the  $\beta$ -hydroxy ester **7** (**42**). From **7**, it was necessary to install an amine at the benzylic position of the indoline core. To accomplish this, we first reduced the ester with  $\text{LiBH}_4$ , followed by protection of the primary alcohol.

Stereoinversion was then accomplished via displacement of the secondary alcohol using diphenylphosphorylazide to furnish an azide, that was next reduced with tin (II) chloride to give the desired primary amine **8**. Installation of our previously optimized oxalamide (**43**) utilizing **9** on the derived primary amine gave intermediate **10**, which was subjected to tetrabutylammonium fluoride to effect removal of the silyl protecting group, followed by Mitsunobu union of the resulting primary alcohol with tri-*N*-bocguanidine to yield intermediate **11**. With these two crucial structural features installed, we turned toward the installation of the methylamino methyl side-chain. Suzuki coupling (**44**) of aryl bromide **11** with potassium vinyltrifluoroborate (**12**), oxidative

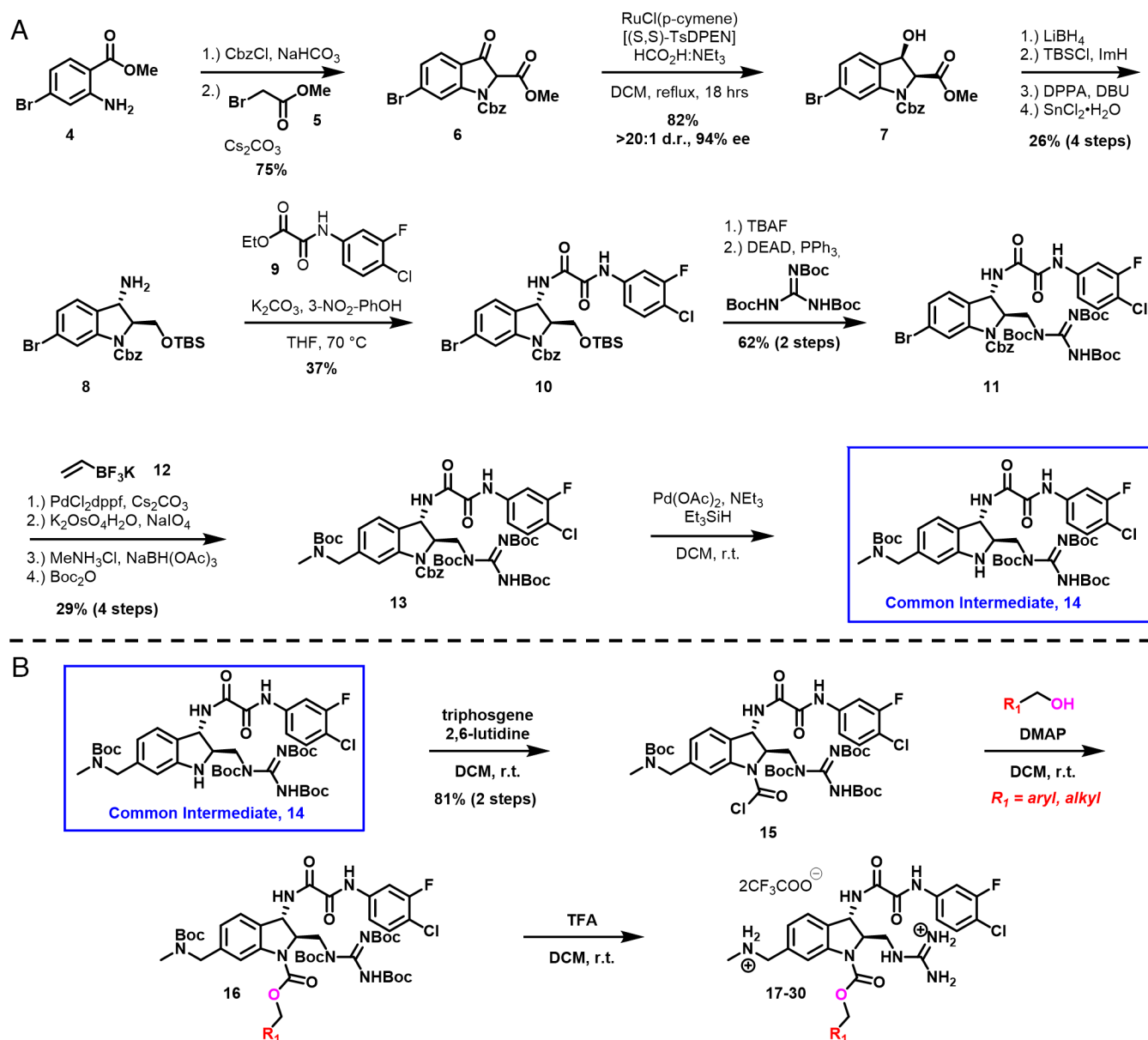


**Fig. 2.** Synthesis of indoline core CD4mcs. (A) Synthetic route toward a common intermediate for analog synthesis starting from commercially available methyl 2-amino-4-bromobenzoate **4**. This route affords the indoline scaffold-containing intermediate **14** in 15 steps and 1.1% overall yield. (B) Functionalization strategy of the common intermediate **14** for analog synthesis.

cleavage, followed by reductive amination of the resulting aldehyde with methylamine, and protection of the free amine as the *tert*-butyl carbamate provided intermediate **13**.

Initially, removal of the benzyl carbamate proved difficult, as employing standard hydrogenation conditions resulted in dechlorination of the *m*-*F*-*p*-Cl aromatic ring. Instead, transfer hydrogenation utilizing Pd(OAc)<sub>2</sub> and Et<sub>3</sub>SiH as the hydride source permitted selective removal of the benzyl carbamate protecting group to give **14**. It should be noted that the indoline scaffold is very sensitive to acidic conditions. Significant transfer of the *tert*-butyloxycarbonyl from the adjacent protected guanidine to the indoline nitrogen was observed even when subjected to weak acids, such as pyridinium hydrochloride. With release of the indoline nitrogen having been achieved, acylation with triphosgene and 2,6-lutidine as base yielded carbamoyl chloride **15**, which proved to be stable, and as such could be used directly without purification in conjunction with various alcohols to produce carbamates such as **16** in excellent yield. Finally, removal of the protecting groups resulted in the carbamates as TFA salts (**17** to **30**, Figs. 2*B* and 3).

Synthetic modifications at the indoline N3 position proceeded with prioritization based on a combination of chemical feasibility, structural considerations, and feedback from viral inhibition assays. Molecular modeling of the CD4mc-gp120 complexes was informed by the disposition of the indane C3 substituent in CJF-III-049-S (**2**), similarity between the indoline and indane scaffolds, and the topography of the gp120 vestibule surface (*SI Appendix*, Figs. S5 and S6). Crystal structures of gp120 complexes with selected compounds tested and refined hypotheses in this structure-based development course.

**B. Inhibition of HIV-1 Infection by Indoline CD4mcs.** Initially, several carbamate analogs were synthesized and tested in an assay measuring the inhibition of single-round HIV-1<sub>JR-FL</sub> infection. We were curious to know if the simplest carbamate (**17**, X = NCO<sub>2</sub>Me) would retain the ability to inhibit Env function. Gratifyingly, this analog displayed a modest 2.5-fold increase in potency (Fig. 3*A*) compared to the previous lead CD4mc, BNM-III-170 (**1**). We also found that indoline **17** bound to gp120 in a similar manner as for indanes **1** and **2**. These results suggested that a wide series of indoline CD4mc warranted further investigation. Carbamates in the alkyl series of ethyl (**18**), propyl (**19**), butyl (**20**), pentyl (**21**), and hexyl (**22**) carbon chain replacements for the methyl group were readily synthesized and tested for inhibition of JR-FL virus pseudotypes (Fig. 3*A*). As the carbon chain length grew, virus inhibition initially increased and then decreased, with peak antiviral activity 24-fold higher than for BNM-III-170 for the three-carbon chain [CJF-III-288 (**19**), Fig. 3*A*].

We also explored the consequences of unsaturated bonds in the carbamate system to see if any effect of addition of an electron pi-cloud could be observed. Allyl carbamate **23** and benzyl carbamate **26** were therefore constructed and tested. The allyl analog **23** proved to be less potent than its propyl counterpart **19**, thus providing no indication of significant pi interactions in the targeted area (Fig. 3*A*). However, the benzyl carbamate **26** demonstrated an 11-fold increase in potency relative to BNM-III-170 (Fig. 3*A*), indicating that the proposed targeted area on Env is sufficient to accommodate an aromatic ring without issue. In general, hydrophobic substituents on the N3-carbamate appear to interact efficiently with the targeted Env region, leading to more potent viral inhibition.

To probe further the structural features of the CD4mc that could increase antiviral potency, we examined the effect of deletion of the one-carbon spacer between the phenyl ring and the

carbamate oxygen in CJF-III-192 (**26**). To this end, the phenyl carbamate derivative **25** was constructed and tested. Interestingly, the antiviral potency of this CD4mc was decreased compared with that of the benzyl carbamate, CJF-III-192 (**26**) (Fig. 3*A*). The crystal structure of CJF-III-192 (**26**) complexed to gp120 (*SI Appendix*, Fig. S1*F* and S3*C*) shows that the one-carbon spacer is essential for providing the rotatable bond needed for the phenyl ring to adopt a favorable binding conformation. Introduction of a *para*-bromine on the phenyl ring of **26** to yield **27** decreased the antiviral activity (Fig. 3*A*); this decrease is not readily explained by the crystal structure of **26**, since the *para* position projects away from gp120 into the solvent.

Allyl carbamate **23** proved useful for analog synthesis as well. A 1,2-diol functionality was readily introduced from the alkene via dihydroxylation. The resulting diol **24** is structurally similar to the indane CD4mc CJF-III-049-S (Fig. 1*C*), but the butanediol substituent is placed further out from the scaffold. A 2.5-fold improvement in viral inhibition by **24** (Fig. 3*A*) compared to BNM-III-170 was observed. These results indicate that **24** is comparable to CJF-III-049-S (**2**) (Fig. 1*C*) in antiviral activity but less active than **23**; therefore, the addition of a diol at this location did not apparently enhance positive interactions with Env.

Selective fluorine incorporation has proved useful in pharmaceutical development (45); we therefore explored such derivatization here for CD4mc indoline compounds. In addition, given the positive effect of 3-substituent hydrophobicity observed in the alkyl and aryl series, we were intrigued by the potential contribution of fluorine incorporation to this effect. Specifically, pentafluorobenzyl carbamate **30**, 1,1,1-trifluoroethyl carbamate **28**, and 1,1,1-trifluoropropyl carbamate **29**, analogs of indolines **26**, **18**, and **19**, respectively, were synthesized and tested for the ability to inhibit HIV-1<sub>JR-FL</sub> infection. The fluorinated analogs **30** and **28** showed 2.1- to 2.7-fold enhanced antiviral activity compared to their respective fully hydrogenated counterparts **26** and **18** (Fig. 3). Pleasingly, the pentafluorobenzyl carbamate in **30** (CJF-IV-046) resulted in a 23-fold improvement in viral inhibition compared to BNM-III-170. The antiviral activity of **29** was similar to that of **19**, indicating that the addition of fluorine did not enhance potency against HIV-1 in this instance. Thus, for some indoline CD4mcs, fluorination can be beneficial to antiviral potency (Fig. 3*A*).

To examine the breadth of the observed antiviral activity, we tested selected indoline CD4mcs against HIV-1<sub>AD8</sub>, a different clade B virus, and against HIV-1<sub>BG505</sub>, a clade A virus that has proven to be more difficult to inhibit with current CD4mcs. The tested indoline CD4mcs (**17–23**, **26–30**) all inhibited HIV-1<sub>AD8</sub> with IC<sub>50</sub> values 3 to 10-fold better than those for HIV-1<sub>JR-FL</sub> (Fig. 3*A*). The clade A HIV-1<sub>BG505</sub> was not susceptible to inhibition by our previous lead CD4mc, BNM-III-170 (**1**, IC<sub>50</sub> > 300 μM) or other tested indane CD4mcs. By contrast, most of the tested indoline CD4mcs inhibited HIV-1<sub>BG505</sub> infection with IC<sub>50</sub> values in the micromolar range (Fig. 3*A*). Of these CD4mcs, CJF-IV-046 (**30**), CJF-III-288 (**19**), CJF-III-192 (**26**), and DY-III-065 (**29**) stood out as the most potent CD4mcs, with BG505 IC<sub>50</sub> values of 10.1 ± 6.8 μM, 27.0 ± 8.8 μM, 31.6 ± 5.7 μM, and 35.0 ± 24.0 μM, respectively. The antiviral IC<sub>50</sub> values of the five most potent indoline CD4mcs and BNM-III-170, as determined in side-by-side assays, are shown in *SI Appendix*, Table S3. To further investigate the underlying binding mechanism of these CD4mcs to HIV-1<sub>BG505</sub>, we then used molecular docking and the free energy of binding calculation using molecular mechanics/generalized born surface area to evaluate binding mode of the CD4mcs and their correlation with experimental IC<sub>50</sub> values (*SI Appendix*, Fig. S5 and S6). These results indicate that the carbamate substituents at

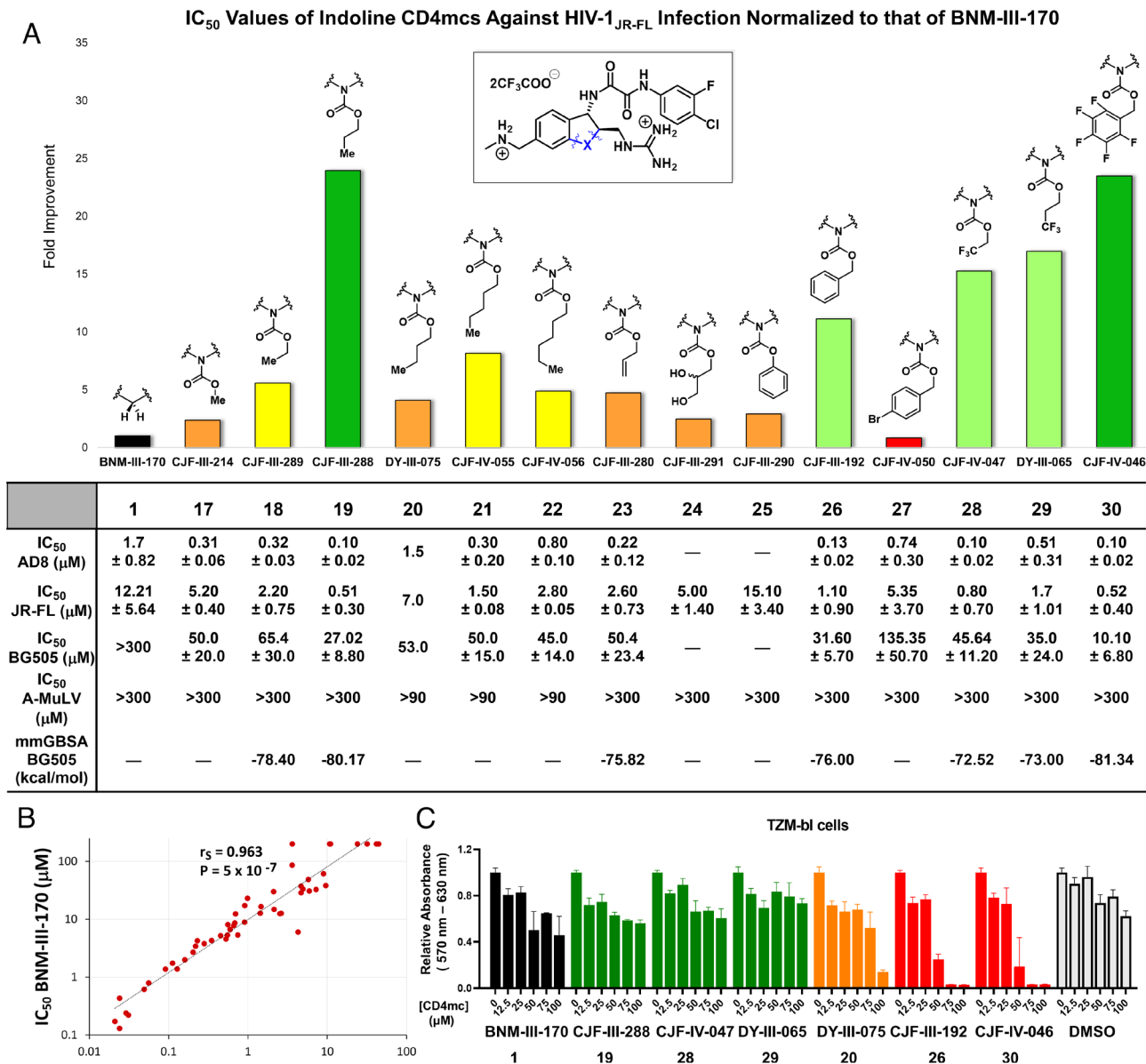


**Fig. 3.** Indoline CD4mcs inhibit HIV-1 entry more effectively than the previous lead indane CD4mc BNM-III-170. (A) Inhibition of infectivity of recombinant HIV-1 pseudotypes by CD4mc analogs. The bar graph shows the inhibitory activity of indoline CD4mcs against infection of recombinant virus pseudotyped with the Env of HIV-1<sub>JR-FL</sub> normalized to that of the IC<sub>50</sub> of BNM-III-170. The table beneath reports the IC<sub>50</sub> values of indoline CD4mcs against viruses pseudotyped with the Envs of the AD8, JR-FL, and BG505 HIV-1 strains. Only three of the compounds (DY-III-075, CJF-IV-055, and CJF-IV-056) inhibited the control virus pseudotyped by the amphotropic murine leukemia virus (A-MLV) Env at concentrations of 300 μM or less. The table also reports the free energy of binding for the indoline CD4mc analogs predicted by an HIV-1<sub>BG505</sub> gp120 docking model. (B) Comparison of the inhibition of infectivity by BNM-III-170 (39) and CJF-III-288 against a panel of recombinant viruses pseudotyped with the Envs of HIV-1 strains from multiple phylogenetic clades. Compared with BNM-III-170, CJF-III-288 displays an approximately 10-fold increase in potency for all HIV-1 pseudotypes examined, with the exception of clade A/E recombinants. Neither BNM-III-170 nor CJF-III-288 inhibited the control virus pseudotyped by the amphotropic murine leukemia virus (A-MLV) Env at concentrations of 100 μM or less. (C) The cell proliferation assay was conducted at varying concentrations of BNM-III-170 and indoline CD4mcs prepared from stock solutions in 100% DMSO (dimethyl sulfoxide). Compounds were incubated with T2M-bl cells for 72 h, after which the relative viability of the cells was evaluated with respect to the cells without treatment. The volume of DMSO used in the DMSO control corresponds to the volume of the CD4mc used at each indicated concentration. Measurements were performed in triplicate. Error bars indicate mean ± SEM. The levels of T2M-bl cell toxicity for the indoline CD4mcs are indicated as minimal (green), moderate (orange), or severe (red).

the indoline N3 nitrogen can confer not only improved potency but also greater breadth against HIV-1 strains.

We next examined the ability of two potent indoline CD4mc analogs, CJF-III-288 (19) and CJF-IV-046 (30), to inhibit infection of T2M-bl target cells by a panel of global HIV-1 strains from phylogenetic clades A, B, C, D, and G, as well as circulating recombinant forms AE, AG, BC, and CD. With the exception of the clade AE HIV-1, which has a His 375 residue that fills the Phe 43 cavity, all of the viruses were inhibited by CJF-III-288 (19) and CJF-IV-046 (30); 92% and 98% of these viruses were inhibited by CJF-III-288 and CJF-IV-046, respectively, with IC<sub>50</sub> values less than 15 μM

(Fig. 3B and *SI Appendix, Table S1*). By contrast, 25% of the viruses were either not inhibited or required more than 15 μM to be inhibited by BNM-III-170 (1). The IC<sub>50</sub> values of BNM-III-170 (1), CJF-III-288 (19), and CJF-IV-046 (30) for this panel of viruses were strongly correlated, with the slope of the regression line indicating an ~10-fold increase in potency for the two indoline CD4mcs over BNM-III-170 (Fig. 3B and *SI Appendix, Table S3* and Fig. S4). These results indicate that the properties of the HIV-1 Env that determine sensitivity/resistance apply to both indane and indoline CD4mcs. A much weaker correlation was observed between the IC<sub>50</sub> values of CJF-III-288 (19) and sCD4-Ig (*SI Appendix, Fig. S4*).

**C. Cytotoxicity of the Indoline CD4mcs.** With the exception of DY-III-075 (**20**), CJF-IV-055 (**21**), and CJF-IV-056 (**22**), none of the indoline CD4mc analogs tested exhibited nonspecific or toxic activity at concentrations up to 300  $\mu\text{M}$  in the antiviral assays using Cf2Th-CD4/CCR5 target cells. However, at concentrations higher than 20  $\mu\text{M}$ , CJF-IV-046 (**30**) exerted nonspecific or toxic effects on the TZM-bl target cells used to evaluate the inhibition of infection by the panel of global HIV-1 strains (*SI Appendix, Table S4*). To investigate potential effects on cell proliferation and viability, the potent indoline CD4mcs **19**, **20**, **26**, **28**, **29**, and **30** and BNM-III-170 were incubated with TZM-bl cells at varying concentrations (Fig. 3C). We observed that CD4mcs bearing aromatic carbamate functionalities (**26** and **30**) inhibited TZM-bl cell proliferation beginning at a concentration of 50  $\mu\text{M}$ . Most of the CD4mcs with alkyl carbamate substituents (**19**, **28**, and **29**) did not affect cell viability; however, at high (100  $\mu\text{M}$ ) concentrations of **20**, toxicity for TZM-bl cells was observed. These results indicate that nonspecific toxicity for TZM-bl cells is associated with indoline analogs with aromatic carbamates, a consideration for future indoline CD4mc design. Fortunately, most alkyl carbamate substituents appear to be nontoxic replacements for the aromatic carbamates, giving rise to CD4mcs that are equally effective in terms of antiviral potency. Moreover, the inclusion of fluorination in the ethyl or propyl carbamates (**28** and **29**) did not adversely affect cell viability. It is worth noting that at higher concentrations, DMSO also decreased the viability of TZM-bl cells.

**D. Crystal Structures of Indoline CD4mcs.** In parallel with indoline CD4mc synthesis and evaluation of antiviral activity, we also analyzed crystal structures of selected compounds in complexes with the HIV-1<sub>C1086</sub> gp120 core<sub>e</sub> protein, which preferentially assumes a CD4-bound conformation (46). Preformed crystals were soaked with individual indoline CD4mcs [CJF-III-214 (**17**), CJF-III-289 (**18**), CJF-III-288 (**19**), CJF-III-192 (**26**), CJF-IV-047 (**28**), DY-III-065 (**29**), or CJF-IV-046 (**30**)], and the atomic structures were refined against X-ray diffraction measurements for the compounds at resolutions from 2.5 to 1.9 Å (*SI Appendix, Table S1*). For comparisons, structures were also redetermined in this P2<sub>1</sub>2<sub>1</sub>2<sub>1</sub> lattice at improved resolution for the previously reported complexes with the indane CD4mcs BNM-III-170 (**39**) and CJF-III-049-S (**38**). Electron density distributions were well-defined, as shown in Fig. 4B for DY-III-065 (**29**) and for each ligand in *SI Appendix, Fig. S1 A–I*. The densities for each of the four copies in the asymmetric unit are highly similar (e.g., *SI Appendix, Fig. S2 A–D* for **29**); accordingly, we constrained the fitted gp120-CD4mc atomic structures to be identical.

Indoline CD4mcs bind to gp120 in a manner typified by DY-III-065 in our best-defined structure at 1.88 Å resolution (Fig. 4A), with interactions like those made by indane CD4mc BNM-III-170 (Fig. 1B). The gp120 binding modes of all seven indoline CD4mcs are the same (Fig. 5A and *SI Appendix, Fig. S3A*), featuring hydrogen-bonding to main-chain carbonyls (Fig. 4B). The substituents at indane positions 1, 2, and 5 of BNM-III-170 (**1**) are preserved identically in CJF-III-049-S (**2**) and in all of the indoline CD4mcs in this study. The methylamino methyl group at C5 makes no gp120 contacts, but the other two are stereo-specifically fixed by hydrogen bonding to the gp120 backbone. Thus, despite varied substitutions at N3 or C3, the binding poses of the indoline CD4mcs are similar to those of the indane CD4mcs (Fig. 5B and *SI Appendix, Fig. S3B*); however, because of geometric differences between the indoline and indane CD4mcs in the dispositions of the fixed C1 and C2 substituents on the five-membered rings, their very similar ring skeletons are oriented differently when bound to gp120 (Fig. 5B). As a consequence, the aromatic six-membered ring is

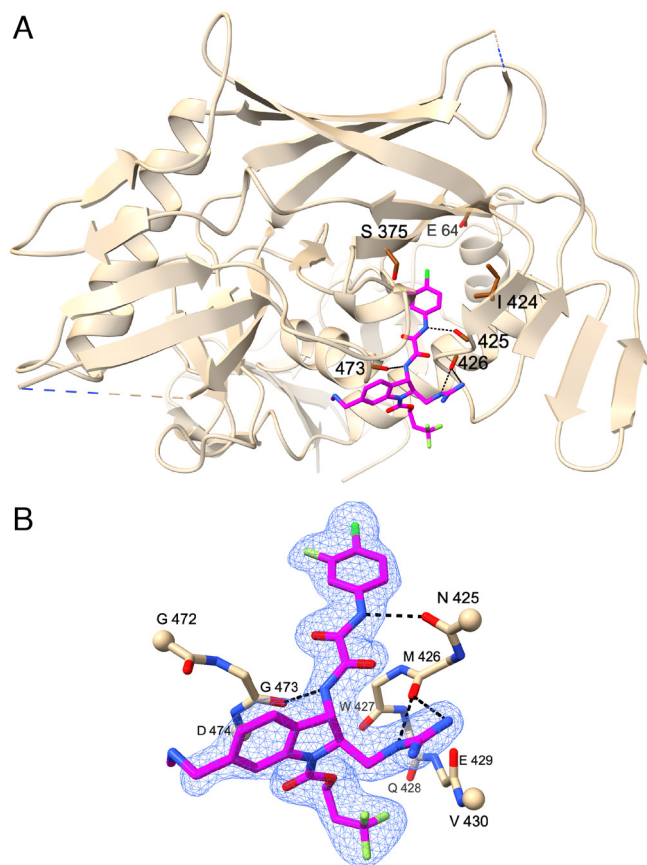


**Fig. 4.** Crystal structure at 1.88 Å resolution of a representative indoline CD4mc, DY-III-065 (**29**), in complex with HIV-1<sub>C1086</sub> gp120 core<sub>e</sub>. (A) DY-III-065 (**29**) in stick representation as complexed with gp120 displayed as a ribbon diagram (beige) and oriented as in Fig. 1A. The carbonyl backbones of residues Asn425, Met426, and Gly473 of gp120 are in stick representation to demonstrate hydrogen bonds with DY-III-065. Hydrogen bonds are shown as black dashed lines. The sites of mutational resistance to indane CD4mc BNM-III-170 (Glu64, Ser375, and Ile424) are also shown in stick representation. The carbon atoms of DY-III-065, carbon atoms of gp120, and the oxygen, nitrogen, chlorine, and fluorine atoms are shown in magenta, brown, red, blue, dark green, and light green, respectively. (B) Crystal structure of DY-III-065 (**29**) as complexed with gp120 displayed in stick representation. The carbon atoms of gp120 are shown in beige. The C<sub>α</sub> atoms of terminal residues in gp120 segments are represented in balls. The electron density is from a 2Fo-Fc synthesis contoured at about 1.5 $\sigma$  and selected for coverage within 2 Å of ligand atoms.

stacked against the G473-D474 peptide unit (Fig. 5C) more closely for the indoline CD4mcs, which should provide greater  $\pi$ - $\pi$  overlap and strengthened binding. Moreover, this redistribution in the indoline CD4mcs (Fig. 5D) relative to the indane CD4mcs (Fig. 5E) also moves several nonbonded contacts into highly favorable van der Waals interactions.

The N3 carbamate ester substituents of the most efficacious indoline CD4mcs studied here (**19**, **29**, and **30**) all occupy spaces in the Phe 43 vestibule of gp120 that are similar to, but distinctive from that for the C3 butanediol substituent of indane CD4mc **2** (Fig. 5E and *SI Appendix, Fig. S3B*). The carbamate ester cores of these indolines are chemically and structurally the same through the first carbon of the carbamate substituent, yet the antiviral activities of these compounds increase from the methyl to propyl, benzyl, trifluoropropyl, and pentafluorobenzyl by factors of 10.2, 4.7, 3.1, and 10.0, respectively. The paucity of gp120 contacts from the carbamate substituents confounds the analysis, especially as compared with those from the C3 substituent in indane **2** (*SI Appendix, Table S2*), which shows more favorable interactions despite having activities >17-fold lower than the best indoline

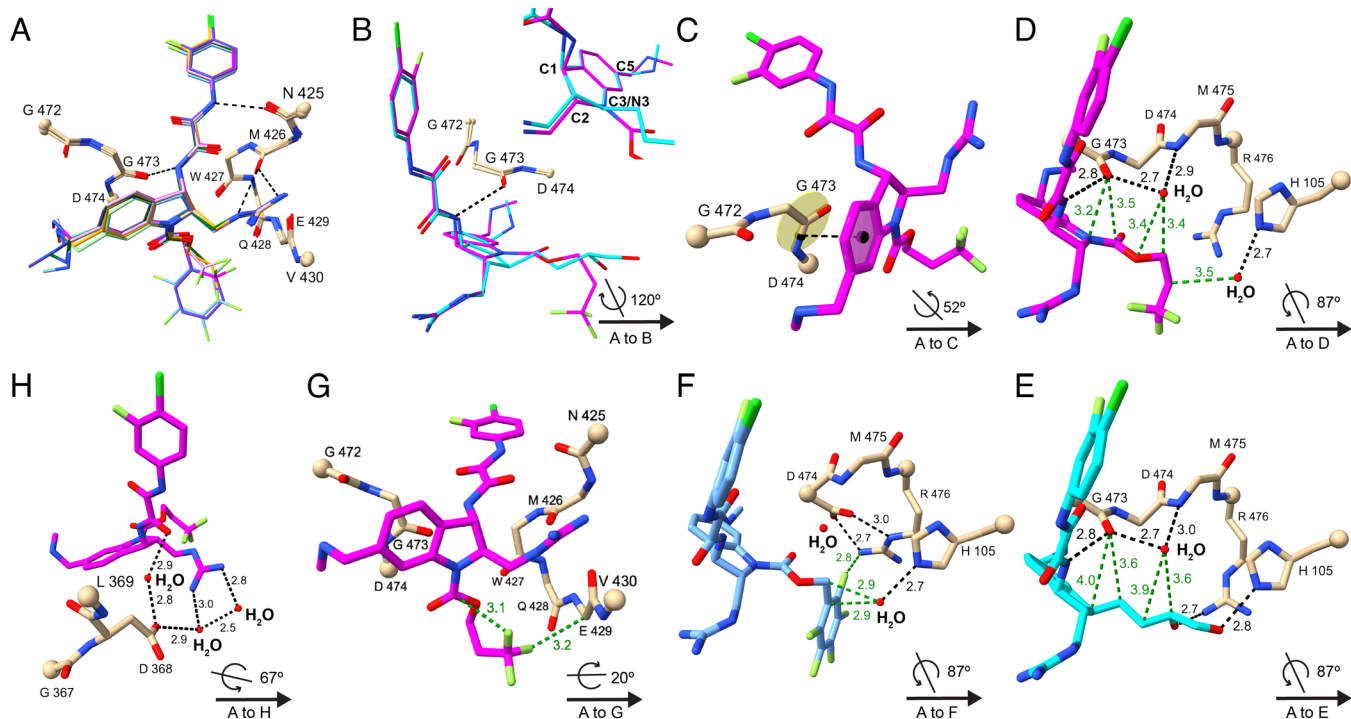


**Fig. 5.** Crystal structures of CD4mcs in complex with HIV-1<sub>C1086</sub> gp120 core<sub>e</sub>. (A) Comparison among crystal structures of indoline CD4mcs after superimposition of the gp120 cores: CJF-III-214 (**17**), light green; CJF-III-289 (**18**), dark green; CJF-III-288 (**19**), orange; CJF-III-192 (**26**), purple; CJF-IV-047 (**28**), pink; DY-III-065 (**29**), magenta; and CJF-IV-046 (**30**), light blue. Carbon atoms of gp120 are in beige; other atoms are colored as in Fig. 4. The C<sub>α</sub> atoms of terminal residues in gp120 segments are represented in balls. A key is given at lower right in each of panels (B)–(H) for the orientation of its structure relative to that of (A). (B) Comparison between indoline CD4mc DY-III-065 (**29**) and indane CD4mc CJF-III-049-S (**2**) after superimposition of the gp120 cores. The carbon atoms of DY-III-065 and CJF-III-049-S are in magenta and cyan, respectively. The inset image compares DY-III-065 and CJF-III-049-S after superimposition of their aromatic six-membered rings. (C)  $\pi$ - $\pi$  interactions between the aromatic six-membered ring of DY-III-065 and the G473-D474 peptide unit of gp120. The black dashed line connects the centroid of the aromatic six-membered ring of DY-III-065 and center of the G473-D474 peptide bond. (D–F) Hydrogen bonds and nonbonded contacts that DY-III-065 (D), CJF-III-049-S (E), or CJF-IV-046 (F) form with gp120 and surrounding water molecules. Hydrogen bonds and nonbonded contacts are shown as black and green dashed lines, respectively. (G) Fluorine atoms of DY-III-065 (**29**) form favored nonbonded contacts with the C<sub>α</sub> of E429 in gp120 and with its own carbamate carbon. (H) A water network at the protein–ligand interface in the structure of the DY-III-065 (**29**) complex associates the strictly conserved gp120 D368 carboxylate with the guanidinium group from C2 of the CD4mc.

CD4mcs (**19**, **29**, and **30**). The benzyl carbamate (**26**) and its pentafluorobenzyl counterpart (**30**) adopt identical conformations as bound to gp120 (*SI Appendix*, Fig. S3C); and the propyl (**19**) and trifluoropropyl (**29**) carbamate are also very similar (*SI Appendix*, Fig. S3D). Thus, the fully hydrogenated and partially fluorinated pairs make very similar gp120 contacts, altogether hydrophobic for the propyl carbamate; nevertheless, fluorine atoms in **30** (Fig. 5F) and **29** (Fig. 5G) participate in contacts with the gp120 core<sub>e</sub> protein.

The structure of the gp120 core<sub>e</sub> complex with DY-III-065 (**29**) reveals water structure at protein–ligand interfaces. One water site, shown in Fig. 5D, is hydrogen-bonded to the carbonyl oxygen of G473, the amino group of M475, and the carbonyl oxygen of W427 (not shown) and just outside hydrogen-bonding distance from the carbamate-linking oxygen atom. A second set of waters associates the C2 guanidinium group of **29** with the carboxyl group of the stringently conserved D368 of gp120, which is critical for CD4 binding (23). The C2 guanidinium nitrogens of **29** H-bond to two water molecules, one of which H-bonds to D368; water-mediated H-bonding also bridges D368 to a C1 oxalamide oxygen of **29** (Fig. 5H). These water sites are also present in the indane CD4mc complexes, but they only become clearly evident here with the highest resolution yet achieved for this system. Synthetic efforts to create new indoline CD4mc analogs that mimic these water-based interactions with D368 are in progress.

It is noteworthy that interactions between DY-III-065 (**29**) and gp120 primarily involve main chain atoms or the side chain of the conserved CD4-binding residue D368 (23, 24). Water

molecules that mediate the contacts between **29** and the side chains of polymorphic HIV-1 gp120 residues (e.g., His/Gln 105) can potentially form hydrogen bonds despite this variation. These characteristics should militate against the evolution of HIV-1 escape mutants.

**E. Antiviral Activity of Indoline CD4mcs against Resistant HIV-1 Variants.** Previously, CD4mc-resistant variants of HIV-1<sub>AD8</sub> were selected by incubating infected cultures with increasing concentrations of BNM-III-170 (**39**). After selection, the derived mutant HIV-1<sub>AD8</sub> 130-C was completely resistant to entry inhibition by concentrations of BNM-III-170 up to 300  $\mu$ M. In this case, two changes in the Phe 43 cavity (I424T and S375N) and a change (E64G) in Layer 1 of the gp120 inner domain individually contributed to BNM-III-170 resistance and acted additively to increase resistance to BNM-III-170 (**39**).

Given the improved breadth of infection inhibition exhibited by the indoline CD4mcs, we were curious if this class of CD4mcs could overcome these resistance-associated adaptations and inhibit the infection of these HIV-1 mutants. The evolved BNM-III-170-resistant HIV-1<sub>AD8</sub> mutant 130-C and the HIV-1<sub>AD8</sub> mutant containing the three resistance-associated gp120 changes (E64G+S375N+I424T) were inhibited by high concentrations of CJF-III-192 (**26**) (Table 1); the CD4mcs CJF-III-288 (**19**) and CJF-IV-046 (**30**) were less effective against these mutants (Table 1). The indoline CD4mcs were also evaluated for their ability to inhibit the HIV-1<sub>AD8</sub> mutants containing single or pairwise combinations of the resistance-associated

**Table 1. Sensitivity of BNM-III-170-resistant HIV-1 variants to inhibition by indoline CD4mcs**

HIV-1(AD8) Env variant	Fold resistance to:				IC50 ( $\mu$ M)		
	BNM-III-170 (1)	CJF-III-288 (19)	CJF-IV-046 (30)	CJF-III-192 (26)	CJF-III-288 (19)	CJF-IV-046 (30)	CJF-III-192 (26)
WT	1	1	1	1	0.20 $\pm$ 0.03	0.20 $\pm$ 0.01	0.20 $\pm$ 0.01
E64G	109	25	20	32.5	5.0 $\pm$ 1.2	4.0 $\pm$ 2.0	6.5 $\pm$ 1.01
S375N	5.2	7.5	8.5	9	1.5 $\pm$ 0.17	1.7 $\pm$ 0.02	1.8 $\pm$ 0.91
I424T	5.2	11	8.5	9	2.2 $\pm$ 0.08	1.7 $\pm$ 0.02	1.8 $\pm$ 0.84
E64G+S375N	>1,500	300	200	200	60.0 $\pm$ 7.2	40.0 $\pm$ 10.0	40.0 $\pm$ 5.0
E64G+I424T	>1,500	375	200	200	75.0 $\pm$ 6.1	40.0 $\pm$ 12.2	40.0 $\pm$ 6.3
S375N+I424T	209	51	41	45	10.1 $\pm$ 2.2	8.2 $\pm$ 2.08	9.0 $\pm$ 3.0
E64G+S375N+I424T	>1,500	1,450	700	650	290.2 $\pm$ 10	140.0 $\pm$ 15.0	130 $\pm$ 35.0
130-C	>1,500	1,305	700	400	260.9 $\pm$ 30	140.0 $\pm$ 20.7	80 $\pm$ 20.0
A-MLV	>1,500	>1,500	>1,500	>1,500	>300	>300	>300

The sensitivity of recombinant luciferase-expressing viruses pseudotyped with the indicated HIV-1<sub>AD8</sub> Env variants to the indoline CD4mcs was determined using Cf2Th-CD4/CCR5 target cells, as described in *Materials and Methods*. The IC<sub>50</sub> values (in  $\mu$ M) are shown in the right three columns. The level of resistance relative to that of the wild-type (WT) AD8 Env is shown in the left columns; the values for the indane CD4mc, BNM-III-170, were derived from ref. 40.

gp120 changes. All of the tested indoline CD4mcs (**19**, **26**, and **30**) inhibited the single-residue HIV-1<sub>AD8</sub> mutants with IC<sub>50</sub> values less than 10  $\mu$ M. The inhibition of infection was diminished for the pairwise combinations of the gp120 changes; however, variants containing all three permutations of the pairwise mutations were still inhibited by the indoline CD4mcs **19**, **26**, and **30** with IC<sub>50</sub> values less than 75  $\mu$ M. In all cases, the indoline CD4mcs were able to inhibit these resistance-selected HIV-1<sub>AD8</sub> mutants more effectively than BNM-III-170 (**39**). Thus, although the gp120 changes that determine resistance to our current lead indane CD4mc, BNM-III-170, also result in relative resistance to the indoline CD4mcs, the increased potency of the indoline CD4mcs allows measurable inhibition of HIV-1 variants that are resistant to BNM-III-170.

**F. ADCC and Antibody Recognition.** CD4mcs have the potential to sensitize HIV-1-infected cells to killing by ADCC (30). We therefore examined the ability of the indoline CD4mc inhibitors: 1) to enhance recognition of Env on the surface of infected cells by antibodies (Ab) present in plasma from HIV-1-infected individuals (HIV+ plasma); 2) to mediate recognition of antibody-bound infected cells by Fc $\gamma$ RIIIa receptors in the presence of HIV+ plasma; and 3) to sensitize infected cells to ADCC mediated by HIV+ plasma. Potent indoline CD4mcs were evaluated first for their ability to enhance HIV+ plasma binding to primary CD4+ T cells infected by HIV-1<sub>JR-FL</sub>. As demonstrated in Fig. 6 *A* and *D*, the indoline CD4mcs CJF-III-288 (**19**), CJF-III-192 (**26**), and CJF-IV-046 (**30**) enhanced the binding of plasma from HIV-1-infected individuals to HIV-1<sub>JR-FL</sub>-infected cells more efficiently than BNM-III-170. We also evaluated whether the CD4mcs were able to enhance HIV+ plasma binding to HIV-1<sub>JR-FL</sub>-infected cells and promote subsequent Fc $\gamma$ RIIIa receptor engagement (Fig. 6 *B* and *E*). All of the indoline CD4mcs examined [CJF-III-288 (**19**), CJF-III-192 (**26**), and CJF-IV-046 (**30**)] improved recombinant soluble dimeric Fc $\gamma$ RIIIa engagement by HIV+ plasma to a greater degree than BNM-III-170. In addition, the indoline CD4mcs CJF-III-288 (**19**), CJF-III-192 (**26**), and CJF-IV-046 (**30**) all enhanced ADCC killing of HIV-1<sub>JR-FL</sub>-infected CD4+ T cells to a greater extent than BNM-III-170 (Fig. 6 *C* and *F*).

In addition to enabling the recognition of HIV-1<sub>JR-FL</sub>-infected CD4+ T-cells by HIV+ plasma, indoline CD4mc CJF-III-288 (**19**) enhanced HIV+ plasma binding to primary CD4+ T cells

infected with a panel of HIV-1 strains ~twofold more effectively than BNM-III-170 (Fig. 6*G*).

## Discussion

CD4mcs are unique small-organic-molecule HIV-1 entry inhibitors that competitively block CD4 binding, trigger premature conformational changes in the Env leading to functional inactivation, and “open” Env, sensitizing virions to antibody neutralization and infected cells to ADCC. Here, we report that certain indoline CD4mc analogs exhibit 10 to 20-fold increases in specific anti-HIV-1 potency, compared with the earlier lead indane CD4mc, BNM-III-170. Accompanying this increase in potency, we observed greater breadth of activity against a range of primary HIV-1 strains. Natural HIV-1 variants exhibit approximately 1,000-fold differences in sensitivity to indane CD4mcs, with a substantial fraction of variants requiring greater than 100  $\mu$ M concentrations of BNM-III-170 to achieve 50% inhibition of infection. Remarkably, regardless of their phylogenetic classification into clade A, B, C, D, AG, BC, or CD, diverse HIV-1 strains exhibited increased sensitivity to the more potent indoline CD4mc analogs. Only clade AE recombinant HIV-1, which has the imidazole side chain of His 375 occupying the Phe 43 cavity, was resistant to potent indoline CD4mcs such as CJF-III-288.

Likewise, an HIV-1<sub>AD8</sub> variant (130-C) selected for resistance to BNM-III-170, as well as recombinant HIV-1 containing key resistance-associated changes in Env, were found to be inhibited more efficiently by the indoline CD4mcs than by BNM-III-170. Apparently, Env changes near or within the Phe 43 cavity (such as S375N and I424T in the 130-C virus) that are unfavorable for CD4mc binding can be compensated by contacts made by the indoline CD4mcs with the gp120 vestibule. These contacts of the indoline CD4mcs also appear to compensate for the more distant E64G change, which may decrease the propensity of Env to stabilize the CD4-bound conformation favored by the CD4mc (40). Thus, although the indoline CD4mcs are still affected by the resistance-associated gp120 changes, the overall increase in the relative antiviral potency of the indoline CD4mcs allows inhibition of the resistant viruses at achievable concentrations.

Although further study is needed, the increased antiviral potency of the indoline CD4mcs, compared with BNM-III-170, likely derives from contacts with the gp120 surface made by the substituents on the N3 nitrogen. Crystal structures suggest that these contacts involve a conserved hydrophobic pocket at the



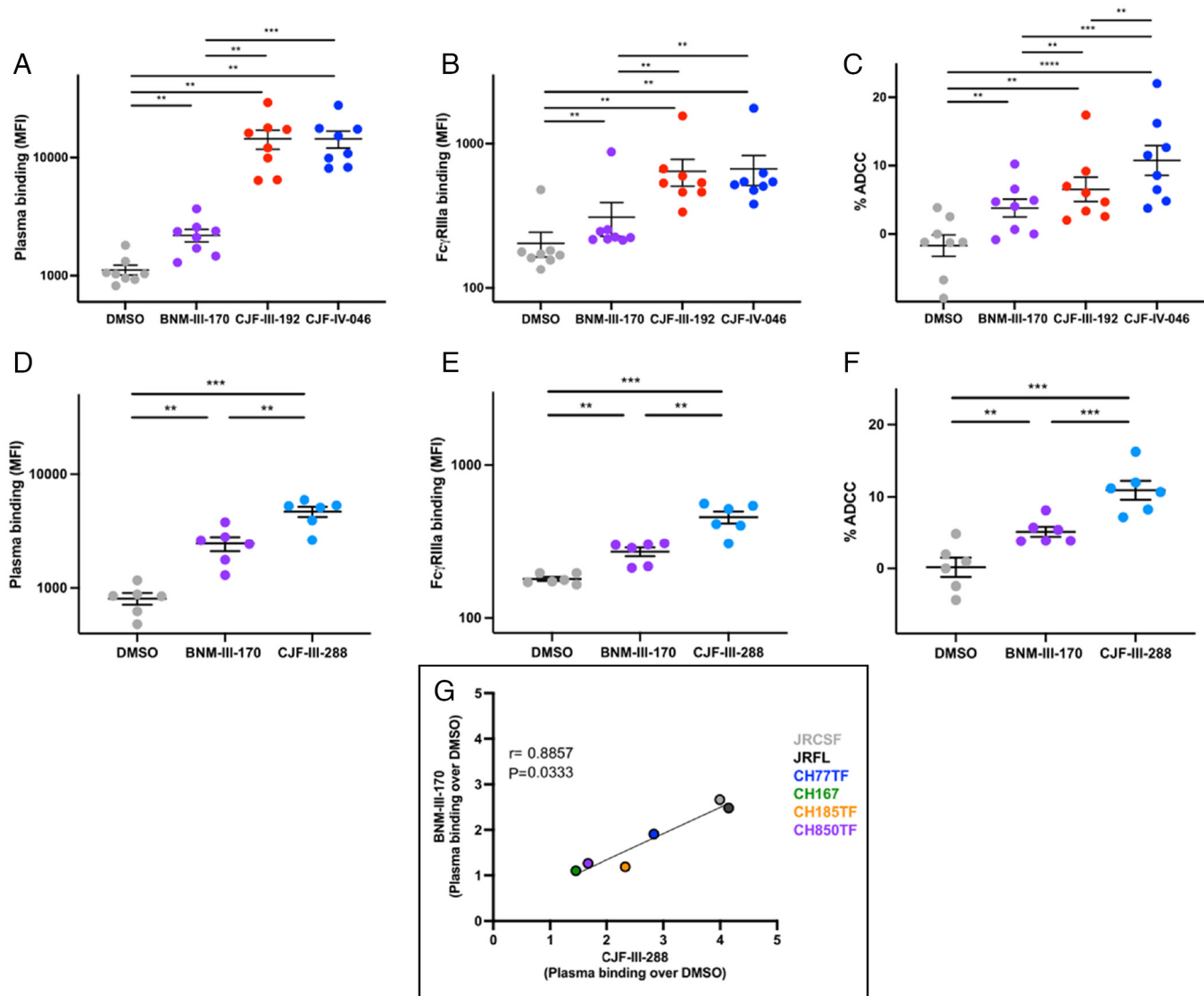


**Fig. 6.** Indoline CD4mcs enhance recognition of HIV-1-infected cells by HIV+ plasma, enabling ADCC. (A–F) Primary CD4+ T cells were infected with HIV-1<sub>JR-FL</sub> and used as targets for HIV+ plasma and Fc $\gamma$ R1IIa binding and for their susceptibility to HIV+ plasma-mediated ADCC. (A) HIV+ plasma binding (MFI) to CD4+ T cells infected with HIV-1<sub>JR-FL</sub> in the presence of DMSO or the indicated CD4mc. (B) Fc $\gamma$ R1IIa binding (MFI) in the presence of HIV+ plasma and DMSO or a CD4mc. (C) HIV+ plasma-mediated ADCC (%) in the presence of DMSO or the indicated CD4mc. (D) HIV+ plasma binding (MFI) in the presence of DMSO or a CD4mc. (E) Fc $\gamma$ R1IIa binding (MFI) in the presence of HIV+ plasma and DMSO or a CD4mc. (F) HIV+ plasma-mediated ADCC (%) in the presence of DMSO or a CD4mc. (G) Comparison of BNM-III-170 and CJF-III-288 stimulation of HIV+ plasma binding to primary CD4+ T cells infected with the indicated HIV-1 strain. Statistical significance was tested using (A–F) paired *t* test or Wilcoxon test based on statistical normality (\*\**P* < 0.01; \*\*\**P* < 0.001 \*\*\*\**P* < 0.0001) and (G) Spearman rank correlation test. Concentrations of CD4mc used in each assay were BNM-III-170 (50  $\mu$ M), CJF-III-192 (50  $\mu$ M), CJF-IV-046 (25  $\mu$ M), or CJF-III-288 (50  $\mu$ M).

junction of the gp120 inner and outer domains (Fig. 1B). This hydrophobic pocket is flanked by the polymorphic residues His/Gln 105 in the  $\alpha$ 1 helix and Arg/Lys 476 in the  $\alpha$ 5 helix. These natural polymorphisms apparently exert only minimal effects on HIV-1 sensitivity to the more potent indoline CD4mcs because several susceptible natural variants exhibit polymorphic changes in these residues. These observations suggest that indoline CD4mc potency may benefit from interactions of the N3 substituent that are tolerant of some natural HIV-1 diversity. A consequence of the additional gp120 contacts made by the N3 substituent may thus be better stabilization of the binding pose shared by the indoline and indane cores. This pose promotes hydrogen bonding with multiple mainchain atoms (Asn 425, Met 426, Trp 427, and Gly 473) that contribute to the ability of CD4mcs to recognize gp120 glycoproteins from multiple strains.

Strong correlations were also observed between the sensitivities of HIV-1 variants to the indane CD4mc BNM-III-170 and to potent

indoline CD4mcs, CJF-III-288, and CJF-IV-046. As the pseudotyped recombinant viruses used in the assays differ only in Env, the observed correlations indicate that Env-specific variables determine sensitivity to CD4mcs in general. The nature of the Env variables accounting for the wide range of sensitivities to CD4mcs is clearly worthy of further investigation. We note that polymorphisms in residues 105 and 476, which can be contacted by some indoline analogs, but not by BNM-III-170, do not result in deviations from the linear correlation in Fig. 3B, supporting the assertion that these natural changes exert minimal impact on the efficacy of the more potent indoline CD4mcs.

Finally, three of the indoline CD4mcs, CJF-III-192, CJF-III-288, and CJF-IV-046, were more effective than BNM-III-170 in exposing vulnerable Env epitopes on the surface of HIV-1-infected cells relevant to ADCC. These results justify ongoing studies in animal models to evaluate the ability of indoline CD4mc to sensitize HIV-1-infected cells to ADCC.

Indoline CD4mcs with improved potency should expedite exploration of the therapeutic and prophylactic potential of these interesting small molecules.

## Materials and Methods

**Ethics Statement.** Written informed consent was obtained from all study participants [the Montreal Primary HIV Infection Cohort (47, 48) and the Canadian Cohort of HIV Infected Slow Progressors (49–51)], and research adhered to the ethical guidelines of CRCHUM and was reviewed and approved by the CRCHUM Institutional Review Board (Ethics Committee, approval number CE 16.164–CA). Research adhered to the standards indicated by the Declaration of Helsinki. All participants were adult and provided informed written consent prior to enrollment in accordance with Institutional Review Board approval.

**Cell Lines and Primary Cells.** 293T cells and TZM-bl cells were grown in Dulbecco's modified Eagle's medium (DMEM) (Life Technologies, Wisent Inc.) supplemented with 10% fetal bovine serum (Life Technologies, VWR) and 100  $\mu\text{g}/\text{mL}$  of penicillin-streptomycin (Life Technologies, Wisent Inc.). Cf2Th cells stably expressing the human CD4 and CCR5 coreceptors for HIV-1 were grown in the same medium supplemented with 0.4 mg/mL of G418 and 0.2 mg/mL of hygromycin.

Human peripheral blood mononuclear cells (PBMCs) from healthy HIV-1-negative individuals were obtained by leukapheresis and Ficoll-Paque density gradient isolation and were cryopreserved in liquid nitrogen until use. CD4+ T lymphocytes were purified from resting PBMCs by negative selection using immunomagnetic beads according to the manufacturer's instructions (StemCell Technologies). The cells were activated with phytohemagglutinin-L (10  $\mu\text{g}/\text{mL}$ ) for 48 h and then maintained in RPMI 1640 complete medium supplemented with recombinant interleukin-2 (100 U/mL).

**Viral Production and Infection.** Vesicular stomatitis virus G-pseudotyped viruses were produced and titrated as previously described (52). Viruses were used to infect activated primary CD4+ T cells from healthy HIV-1-negative donors by spin infection at  $800\times g$  for 1 h in 96-well plates at 25  $^{\circ}\text{C}$ .

**CD4-Mimetic Compounds (CD4mcs).** The CD4mc analogs were synthesized as described in detail in the *SI Appendix*. The compounds were dissolved in DMSO at a stock concentration of 10 mM and stored at  $-20^{\circ}\text{C}$  until use. The CD4mcs were diluted to 1 mM in DMEM for pseudovirus inhibition assays, 50 or 25  $\mu\text{M}$  in PBS for cell-surface staining, and 50 or 25  $\mu\text{M}$  in RPMI 1640 complete medium for ADCC assays.

**Antibodies and Plasma.** The sCD4-Ig used in the virus inhibition assays is described in ref. 40. The anti-coreceptor binding site 17b monoclonal antibody (mAb) (NIH HIV Reagent Program) and plasma from HIV-1-infected individuals were used to assess cell-surface Env conformation. Plasma from the Montreal Primary HIV Infection Cohort (47, 48) and the Canadian Cohort of HIV Infected Slow Progressors (49–51) were collected, heat-inactivated, and conserved at  $-80^{\circ}\text{C}$  until use. The conformation-independent anti-gp120 outer-domain 2G12 mAb (NIH HIV Reagent Program) was used to normalize Env expression. Goat anti-human IgG (H+L) (Thermo Fisher Scientific) antibodies precoupled to Alexa Fluor 647 and streptavidin conjugated to Alexa Fluor 647 were used as a secondary antibody in flow cytometry experiments.

**Inhibition of HIV-1 Infection by CD4mcs.** HIV-1 inhibition assays were performed as described previously (29, 40, 43). To produce recombinant luciferase-expressing HIV-1, 293T cells were transfected with plasmids expressing HIV-1 Env variants and Rev, the pCMV $\Delta$ P1 $\Delta$ env HIV-1 Gag-Pol packaging construct, and the firefly luciferase-expressing HIV-1 vector at a 1:1:3  $\mu\text{g}$  DNA ratio using Effectene transfection reagent (Qiagen). Recombinant luciferase-expressing viruses capable of a single round of replication were released into the cell medium and were harvested 48 h later. The virus-containing supernatants were clarified by low-speed centrifugation ( $600\times g$  for 10 min) and used for single-round infections. To measure the inhibition of infection, the recombinant viruses were incubated with the CD4mcs for 1 h at 37  $^{\circ}\text{C}$ . The mixture was then added to Cf2Th-CD4/CCR5 target cells expressing CD4 and CCR5. After 48 h of culture, the target cells were lysed and the luciferase activity was measured. The relative infectivity was calculated by dividing the luciferase activity by that observed for the same virus

in the absence of the CD4mc. The concentrations of CD4mc ( $\text{IC}_{50}$  values) that inhibit 50% of infection were determined by fitting the data in five-parameter dose-response curves using GraphPad Prism. The reported  $\text{IC}_{50}$  values represent the means and SDs derived from at least two independent experiments, typically with three parallel measurements within an assay.

The pseudotyped virus inhibition assays used to generate the data in Fig. 3B and *SI Appendix, Table S1* were conducted as previously described (39). Single-round HIV-1 pseudotyped by the Envs from a panel of multiclade HIV-1 were incubated for 1 h at 37  $^{\circ}\text{C}$  with fivefold serial dilutions of CD4mc or sCD4-Ig in duplicate. TZM-bl cells were then added in growth medium containing DEAE-dextran at a final concentration of 11  $\mu\text{g}/\text{mL}$ . The assay plates were incubated for 48 h at 37  $^{\circ}\text{C}$ , 5%  $\text{CO}_2$ , after which the cells were lysed and luciferase reporter gene expression was measured using Bright-Glo luciferase reagent (Promega) and a Victor 3 or GloMax Navigator luminometer (Perkin Elmer/Promega). The 50% and 80% inhibitory concentrations ( $\text{IC}_{50}$  and  $\text{IC}_{80}$ , respectively) were calculated based on the relative luciferase unit (RLU) activity in the treated sample compared with that in the untreated control, after subtraction of the background RLU in control uninfected TZM-bl cells.

**Cell Viability Assay.** TZM-bl cells were seeded in 96-well assay plates containing 100  $\mu\text{L}$  of culture medium. CD4mcs in stock solutions of 100% DMSO were added at the specified final concentrations in triplicates. For the DMSO control, a volume of DMSO was added that corresponded to the volume of the CD4mc added at each indicated concentration. After 72 h, cell viability was measured using the CellTiter 96<sup>®</sup> Non-Radioactive Cell Proliferation Assay [(3-(4,5-dimethylthiazol-2-yl)-2,5-diphenyltetrazolium bromide) (MTT)] kit from Promega. Briefly, 15  $\mu\text{L}$  of dye solution (from the kit) was added to each well followed by incubation of the plate at 37  $^{\circ}\text{C}$  for 4 h in a humidified  $\text{CO}_2$  incubator. One hundred  $\mu\text{L}$  of solubilization/stop solution (from the kit) was then added to each well. Absorbance at 570 nm and 630 nm was measured using a 96-well plate reader.

**Flow Cytometry Analysis of Cell-Surface Staining.** Cell surface staining of primary infected cells was performed 48 h postinfection as previously described (30). HIV-1-infected cells were incubated for 1 h at 37  $^{\circ}\text{C}$  with HIV+ plasma (1:1,000 dilution) in the presence of CD4mcs (25 or 50  $\mu\text{M}$ ) or with equivalent volume of vehicle (DMSO). Cells were then washed once with PBS and stained with appropriate Alexa Fluor-647-conjugated (Invitrogen) secondary Abs (2  $\mu\text{g}/\text{mL}$ ) for 20 min at room temperature. Alternatively, the binding of HIV+ plasma was detected using a biotin-tagged dimeric recombinant soluble Fc $\gamma$ RIIIa (0.2  $\mu\text{g}/\text{mL}$ ) followed by the addition of Alexa Fluor 647-conjugated streptavidin (Thermo Fisher Scientific; 2  $\mu\text{g}/\text{mL}$ ). Infected cells were then stained intracellularly for HIV-1 p24, using the Cytofix/Cytoperm Fixation/ Permeabilization Kit (BD Biosciences, Mississauga, ON, Canada) and the fluorescent anti-p24 mAb (PE or FITC-conjugated anti-p24, clone KC57; Beckman Coulter/Immunotech). The percentage of infected cells (p24+ cells) was determined by gating the living cell population on the basis of AquaVivid viability dye staining. Samples were analyzed on an LSRII cytometer (BD Biosciences), and data analysis was performed using FlowJo vX.0.7 (Tree Star, Ashland, OR, USA).

**ADCC FACS-Based Assay.** Measurement of ADCC using the FACS-based assay was performed at 48 h postinfection as previously described (30, 34). Briefly, HIV-1<sub>JR-FL</sub>-infected primary CD4+ T cells were stained with viability (AquaVivid; Thermo Fisher Scientific) and cellular (cell proliferation dye eFluor670; eBioscience) markers and used as target cells. Autologous PBMC effector cells, stained with another cellular marker (cell proliferation dye eFluor450; eBioscience), were added at an effector: target ratio of 10:1 in 96-well V-bottom plates (Corning, Corning, NY). Briefly, infected primary CD4+ T cells were incubated with HIV+ plasma (1:1,000), in the presence of CD4mcs (25 or 50  $\mu\text{M}$ ) or an equivalent volume of vehicle (DMSO). The plates were subsequently centrifuged for 1 min at 300 g and incubated at 37  $^{\circ}\text{C}$ , 5%  $\text{CO}_2$  for 4 to 6 h before being fixed in a 2% PBS-formaldehyde solution. Cells were then stained intracellularly for HIV-1 p24 as described above. Samples were analyzed on an LSRII cytometer (BD Biosciences). Data analysis was performed using FlowJo vX.0.7 (Tree Star). The percentage of ADCC was calculated with the following formula: (% of p24+ cells in Targets plus Effectors) – (% of p24+ cells in Targets plus Effectors plus plasma)/(% of p24+ cells in Targets) by gating on infected live target cells.

**Statistical Analysis.** Statistics were analyzed using GraphPad Prism version 9.4.1 (GraphPad, San Diego, CA, USA). Every dataset was tested for statistical

normality, and this information was used to apply the appropriate (parametric or nonparametric) statistical test. *P* values < 0.05 were considered significant; significance values are indicated as \**P* < 0.05, \*\**P* < 0.01, \*\*\**P* < 0.001, \*\*\*\**P* < 0.0001.

**Protein Purification and X-ray Crystallography.** The plasmid expressing the gp120 core<sub>e</sub> protein of the clade C HIV-1<sub>1086</sub> was donated by Lei Chen from Peter Kwong's laboratory (NIH) (46). An 8-histidine (8His) tag was added to the C-terminus of the gp120 core<sub>e</sub> protein to assist affinity purification. About 1 mg of the expressor plasmid was transfected into 1 L of HEK293S GnTI- suspension cells at  $2 \times 10^6$  cells/mL. After expression of the core<sub>e</sub> protein, the supernatant was filtered using a 0.45- $\mu$ m filter and passed through a prepacked Ni-NTA column. The Ni-NTA column was washed with 40 mM imidazole in  $1 \times$  phosphate-buffered saline (PBS) and the 8His-tagged gp120 core<sub>e</sub> protein was eluted with 250 mM imidazole in  $1 \times$  PBS. The eluted gp120 core<sub>e</sub> protein was deglycosylated overnight in a 37 °C water bath with Endoglycosidase Hf (New England Biolabs). Afterward, the deglycosylated gp120 was further purified using Concanavalin A (Con A)-Sepharose (Cytiva) to remove any incompletely deglycosylated proteins. The flowthrough of the Con A-Sepharose column was collected and further purified using a prepacked Ni-NTA column, which removed Endoglycosidase Hf in the flowthrough. The completely deglycosylated gp120 core<sub>e</sub> protein was eluted with 250 mM imidazole in  $1 \times$  PBS and further polished with a Superdex 200 Increase column (Cytiva). The purified deglycosylated gp120 core<sub>e</sub> protein was concentrated to 10 mg/mL for crystallization.

Crystallization of the unliganded gp120 core<sub>e</sub> protein was performed at 20 °C using the hanging drop vapor diffusion method. The crystals grew in drops consisting of 1  $\mu$ L of protein solution and 1  $\mu$ L of reservoir solution to equilibrate against 600  $\mu$ L of reservoir solution 14 to 16 % (w/v) polyethylene glycol (PEG) 1500, 0.1 M CaCl<sub>2</sub>, 0.1 M imidazole pH 6.5. For each experiment, the compound of interest was dissolved in 100% DMSO. A single crystal was picked from the mother liquor and soaked in 5  $\mu$ L of a stabilization buffer that contained 26% PEG 1500 (w/v), 0.1 M CaCl<sub>2</sub>, 0.1 M imidazole pH 6.5, 2.5 mM Tris-HCl pH 7.5, 350 mM NaCl, 0.02% NaN<sub>3</sub>, 5% (v/v) DMSO, and 2 mM of the compound. The gp120 core<sub>e</sub> crystals were soaked for 30 to 60 min in the stabilization buffer and then transferred for 5 s in cryoprotectant, which is the stabilization buffer but with 30% ethylene glycol. Diffraction data were collected on 24ID-C and 24ID-E beamline at Advanced Photon Source (APS) at Argonne National Laboratory. Crystal

structures were solved by the molecular replacement module in PHENIX using the unliganded HIV-1C<sub>1086</sub> gp120 core<sub>e</sub> structure (PDB ID: 3TGR) and refined with phenix.refine.

**Data, Materials, and Software Availability.** Atomic coordinates and structure factors have been deposited in the Research Collaboratory for Structural Bioinformatics (RCSB) Protein Data Bank, [www.rcsb.org](http://www.rcsb.org) under accession code 8FLY for BNM-III-170 (53), 8FLZ for CJF-III-049-S (54), 8FMO for CJF-III-214 (55), 8FM2 for CJF-III-289 (56), 8FM3 for CJF-III-288 (57), 8FM4 for CJF-IV-047 (58), 8FM5 for DY-III-065 (59), 8FM7 for CJF-III-192 (60), and 8FM8 for CJF-IV-046 (61).

**ACKNOWLEDGMENTS.** We thank Irwin Chaiken and other project leaders of the P01 Consortium Structure-Based Antagonism of HIV-1 Envelope Function in Cell Entry (NIH Grant No. AI 150471). We also thank the staff at Northeastern Collaborative Access Team (NE-CAT) beamlines at Advanced Photon Source (APS) for their support during data collection. We also acknowledge Dr. Charles Ross and Dr. Jun Gu (University of Pennsylvania) for their assistance in obtaining mass and NMR spectra, respectively. We also thank Dr. Mark Hogarth for kindly providing recombinant dimeric Fc $\gamma$ RIIIa and Dr. Beatrice Hahn for providing the following infectious molecular clones: HIV<sub>CH77TF</sub>, HIV<sub>CH185TF</sub>, HIV<sub>CH850TF</sub>, and HIV<sub>CH167</sub>. A.F. is the recipient of a Canada Research Chair on Retroviral Entry #RCHS0235 950-232424.

Author affiliations: <sup>a</sup>Department of Chemistry, University of Pennsylvania, Philadelphia, PA 19104; <sup>b</sup>Department of Cancer Immunology and Virology, Dana-Farber Cancer Institute, Harvard Medical School, Boston, MA 02115; <sup>c</sup>Department of Microbiology, Harvard Medical School, Boston, MA 02115; <sup>d</sup>Department of Biochemistry and Molecular Biophysics, Columbia University, New York, NY 10032; <sup>e</sup>Department of Chemical and Biological Engineering, Drexel University, Philadelphia, PA 19104; <sup>f</sup>Centre de Recherche du CHUM, Montreal, QC H2X 0A9, Canada; <sup>g</sup>Département de Microbiologie, Infectiologie et Immunologie, Université de Montreal, Montreal, QC H3T 1J4, Canada; <sup>h</sup>Center for Virology and Vaccine Research, Beth Israel Deaconess Medical Center, Boston, MA 02215; <sup>i</sup>Department of Physiology and Cellular Biophysics, Columbia University, New York, NY 10032; and <sup>j</sup>Department of Immunology and Infectious Diseases, Harvard School of Public Health, Boston, MA 02115

Author contributions: C.J.F., S.A., Z.G., M.S.S., N.M., C.A., A.F., W.A.H., J.G.S., and A.B.S. designed research; C.J.F., S.A., Z.G., M.M., J.R., C.B., K.T.S., H.R., D.Y., H.-C.C., and T.-J.C. performed research; C.J.F., S.A., Z.G., M.M., J.R., C.B., D.Y., H.-C.C., T.-J.C., M.S.S., N.M., C.A., A.F., W.A.H., J.G.S., and A.B.S. analyzed data; and C.J.F., S.A., Z.G., A.F., W.A.H., J.G.S., and A.B.S. wrote the paper.

- UNAIDS, "Global HIV & AIDS statistics – Fact sheet" (United Nations, 2021).
- S. P. Eholié, F. E. Aoussi, I. S. Ouattara, E. Bissagnéné, X. Anglaret, HIV treatment and care in resource-constrained environments: Challenges for the next decade. *J. Int. AIDS Soc.* **15**, 17334 (2012).
- S. G. Deeks, J. Overbaugh, A. Phillips, S. Buchbinder, HIV infection. *Nat. Rev. Disease Primers* **1**, 15035 (2015).
- R. Wyatt, J. Sodroski, The HIV-1 envelope glycoproteins: Fusogens, antigens, and immunogens. *Science* **280**, 1884–1888 (1998).
- W. G. Robey *et al.*, Characterization of envelope and core structural gene products of HTLV-III with sera from AIDS patients. *Science* **228**, 593–595 (1985).
- J. S. Allan *et al.*, Major glycoprotein antigens that induce antibodies in AIDS patients are encoded by HTLV-III. *Science* **228**, 1091–1094 (1985).
- B. F. Haynes *et al.*, HIV-Host interactions: Implications for vaccine design. *Cell Host & Microbe* **19**, 292–303 (2016).
- A. S. Fauci, An HIV vaccine: Mapping uncharted territory. *JAMA* **316**, 143–144 (2016).
- J. A. Hoxie, Toward an antibody-based HIV-1 vaccine. *Annu. Rev. Med.* **61**, 135–152 (2010).
- G. B. Karlsson Hedestam *et al.*, The challenges of eliciting neutralizing antibodies to HIV-1 and influenza virus. *Nat. Rev. Microbiol.* **6**, 143–155 (2008).
- J. Richard, J. Prévost, N. Alsaifi, S. Ding, A. Finzi, Impact of HIV-1 envelope conformation on ADCC responses. *Trends Microbiol.* **26**, 253–265 (2018).
- J. B. Munro *et al.*, Conformational dynamics of single HIV-1 envelope trimers on the surface of native virions. *Science* **346**, 759 (2014).
- A. Herschhorn *et al.*, Release of gp120 restraints leads to an entry-competent intermediate state of the HIV-1 envelope glycoproteins. *mBio* **7**, e01598-16 (2016).
- X. Ma *et al.*, HIV-1 Env trimer opens through an asymmetric intermediate in which individual protomers adopt distinct conformations. *eLife* **7**, e34271 (2018).
- H. Haim *et al.*, Contribution of intrinsic reactivity of the HIV-1 envelope glycoproteins to CD4-independent infection and global inhibitor sensitivity. *PLoS Pathogens* **7**, e1002101 (2011).
- X. Wei *et al.*, Antibody neutralization and escape by HIV-1. *Nature* **422**, 307–312 (2003).
- C. B. Wilen, J. C. Tilton, R. W. Doms, Molecular mechanisms of HIV entry. *Adv. Exp. Med. Biol.* **726**, 223–242 (2012).
- G. B. Melikyan *et al.*, Evidence that the transition of HIV-1 gp41 into a six-helix bundle, not the bundle configuration, induces membrane fusion. *J. Cell Biol.* **151**, 413–423 (2000).
- S. E. Kuhmann, E. J. Platt, S. L. Kozak, D. Kabat, Cooperation of multiple CCR5 coreceptors is required for infections by human immunodeficiency virus type 1. *J. Virol.* **74**, 7005–7015 (2000).
- W. Weissenhorn, A. Dessen, S. C. Harrison, J. J. Skehel, D. C. Wiley, Atomic structure of the ectodomain from HIV-1 gp41. *Nature* **387**, 426–430 (1997).
- D. C. Chan, D. Fass, J. M. Berger, P. S. Kim, Core structure of gp41 from the HIV envelope glycoprotein. *Cell* **89**, 263–273 (1997).
- M. Lu, S. C. Blacklow, P. S. Kim, A trimeric structural domain of the HIV-1 transmembrane glycoprotein. *Nat. Struct. Biol.* **2**, 1075–1082 (1995).
- P. D. Kwong *et al.*, Structure of an HIV gp120 envelope glycoprotein in complex with the CD4 receptor and a neutralizing human antibody. *Nature* **393**, 648–659 (1998).
- R. Wyatt *et al.*, The antigenic structure of the HIV gp120 envelope glycoprotein. *Nature* **393**, 705–711 (1998).
- J. R. Courter *et al.*, Structure-based design, synthesis and validation of CD4-mimetic small molecule inhibitors of HIV-1 entry: Conversion of a viral entry agonist to an antagonist. *Acc. Chem. Res.* **47**, 1228–1237 (2014).
- A. Schön *et al.*, Thermodynamics of binding of a low-molecular-weight CD4 mimetic to HIV-1 gp120. *Biochemistry* **45**, 10973–10980 (2006).
- Q. Zhao *et al.*, Identification of N-phenyl-N'-(2,2,6,6-tetramethyl-piperidin-4-yl)-oxalamides as a new class of HIV-1 entry inhibitors that prevent gp120 binding to CD4. *Virology* **339**, 213–225 (2005).
- H. Haim *et al.*, Soluble CD4 and CD4-mimetic compounds inhibit HIV-1 infection by induction of a short-lived activated state. *PLoS Pathogens* **5**, e1000360 (2009).
- N. Madani *et al.*, Activation and inactivation of primary human immunodeficiency virus envelope glycoprotein trimers by CD4-mimetic compounds. *J. Virol.* **91**, e01880-16 (2017).
- J. Richard *et al.*, CD4 mimetics sensitize HIV-1-infected cells to ADCC. *Proc. Natl. Acad. Sci. U.S.A.* **112**, E2687 (2015).
- N. Madani *et al.*, CD4-mimetic small molecules sensitize human immunodeficiency virus to vaccine-elicited antibodies. *J. Virol.* **88**, 6542–6555 (2014).
- K. Yoshimura *et al.*, Enhanced exposure of human immunodeficiency virus type 1 primary isolate neutralization epitopes through binding of CD4 mimetic compounds. *J. Virol.* **84**, 7558–7568 (2010).
- S. Ding *et al.*, Short communication: Small-molecule CD4 mimetics sensitize HIV-1-infected cells to antibody-dependent cellular cytotoxicity by antibodies elicited by multiple envelope glycoprotein immunogens in nonhuman primates. *AIDS Res. Hum. Retroviruses* **33**, 428–431 (2017).
- S. Ding *et al.*, A new family of small-molecule CD4-mimetic compounds contacts highly conserved aspartic acid 368 of HIV-1 gp120 and mediates antibody-dependent cellular cytotoxicity. *J. Virol.* **93**, e01325-19 (2019).

35. J. K. Rajashekar *et al.*, Modulating HIV-1 envelope glycoprotein conformation to decrease the HIV-1 reservoir. *Cell Host & Microbe*. **29**, 904–916. e906 (2021).
36. N. Madani *et al.*, A CD4-mimetic compound enhances vaccine efficacy against stringent immunodeficiency virus challenge. *Nat. Commun.* **9**, 2363 (2018).
37. A. M. Princiotto *et al.*, A small-molecule CD4-Mimetic compound protects bone marrow–liver–thymus humanized mice from HIV-1 infection. *J. Infect. Dis.* **218**, 471–475 (2018).
38. C. J. Fritschi *et al.*, Identification of gp120 residue His105 as a novel target for HIV-1 neutralization by small-molecule CD4-mimics. *ACS Med. Chem. Lett.* **12**, 1824–1831 (2021).
39. B. Melillo *et al.*, Small-molecule CD4-mimics: Structure-based optimization of HIV-1 entry inhibition. *ACS Med. Chem. Lett.* **7**, 330–334 (2016).
40. S. Anang *et al.*, Characterization of human immunodeficiency virus (HIV-1) envelope glycoprotein variants selected for resistance to a CD4-mimetic compound. *J. Virol.* **96**, e0063622 (2022).
41. J. Chen *et al.*, Development of an effective scalable enantioselective synthesis of the HIV-1 entry inhibitor BNM-III-170 as the bis-trifluoroacetate salt. *Organic Process Res. Dev.* **23**, 2464–2469 (2019).
42. Z. Luo *et al.*, Stereogenic cis-2-substituted-N-acetyl-3-hydroxy-indolines via ruthenium(II)-catalyzed dynamic kinetic resolution–Asymmetric transfer hydrogenation. *Chem. Commun.* **54**, 13503–13506 (2018).
43. N. Madani *et al.*, Small-molecule CD4 mimics interact with a highly conserved pocket on HIV-1 gp120. *Structure* **16**, 1689–1701 (2008).
44. N. Miyaura, K. Yamada, A. Suzuki, A new stereospecific cross-coupling by the palladium-catalyzed reaction of 1-alkenylboranes with 1-alkenyl or 1-alkynyl halides. *Tetrahedron Lett.* **20**, 3437–3440 (1979).
45. K. Müller, C. Faeh, F. Diederich, Fluorine in pharmaceuticals: Looking beyond intuition. *Science* **317**, 1881–1886 (2007).
46. Y. D. Kwon *et al.*, Unliganded HIV-1 gp120 core structures assume the CD4-bound conformation with regulation by quaternary interactions and variable loops. *Proc. Natl. Acad. Sci. U.S.A.* **109**, 5663–5668 (2012).
47. J. Fontaine, J. Chagnon-Choquelet, H. S. Valcke, J. Poudrier, M. Roger, High expression levels of B lymphocyte stimulator (BlyS) by dendritic cells correlate with HIV-related B-cell disease progression in humans. *Blood* **117**, 145–155 (2011).
48. J. Fontaine *et al.*, HIV infection affects blood myeloid dendritic cells after successful therapy and despite nonprogressing clinical disease. *J. Infect. Dis.* **199**, 1007–1018 (2009).
49. F. Pereyra *et al.*, The major genetic determinants of HIV-1 control affect HLA class I peptide presentation. *Science* **330**, 1551–1557 (2010).
50. P. Kanya *et al.*, Receptor-ligand requirements for increased NK cell polyfunctional potential in slow progressors infected with HIV-1 coexpressing KIR3DL1\*H/\*Y and HLA-B\*57. *J. Virol.* **85**, 5949–5960 (2011).
51. Y. Peretz *et al.*, Functional T cell subsets contribute differentially to HIV peptide-specific responses within infected individuals: Correlation of these functional T cell subsets with markers of disease progression. *Clin. Immunol. (Orlando, Fla.)* **124**, 57–68 (2007).
52. J. Prévost *et al.*, The HIV-1 Env gp120 inner domain Shapes the Phe43 cavity and the CD4 binding site. *mBio* **11**, e00280-20 (2020).
53. Z. Gong, HIV-1 gp120 complex with BNM-III-170. Protein Data Bank. <https://www.rcsb.org/structure/unreleased/8FLY>. Deposited 22 December 2022.
54. Z. Gong, HIV-1 gp120 complex with CJF-III-049-S. Protein Data Bank. <https://www.rcsb.org/structure/unreleased/8FLZ>. Deposited 22 December 2022.
55. Z. Gong, HIV-1 gp120 complex with CJF-III-214. Protein Data Bank. <https://www.rcsb.org/structure/unreleased/8FM0>. Deposited 22 December 2022.
56. Z. Gong, HIV-1 gp120 complex with CJF-III-289. Protein Data Bank. <https://www.rcsb.org/structure/unreleased/8FM2>. Deposited 22 December 2022.
57. Z. Gong, HIV-1 gp120 complex with CJF-III-288. Protein Data Bank. <https://www.rcsb.org/structure/unreleased/8FM3>. Deposited 22 December 2022.
58. Z. Gong, HIV-1 gp120 complex with CJF-IV-047. Protein Data Bank. <https://www.rcsb.org/structure/unreleased/8FM4>. Deposited 22 December 2022.
59. Z. Gong, HIV-1 gp120 complex with DY-III-065. Protein Data Bank. <https://www.rcsb.org/structure/unreleased/8FM5>. Deposited 22 December 2022.
60. Z. Gong, HIV-1 gp120 complex with CJF-III-192. Protein Data Bank. <https://www.rcsb.org/structure/unreleased/8FM7>. Deposited 22 December 2022.
61. Z. Gong, HIV-1 gp120 complex with CJF-IV-046. Protein Data Bank. <https://www.rcsb.org/structure/unreleased/8FM8>. Deposited 22 December 2022.